Current Research in Pharmacology and Drug Discovery 3 (2022) 100084

Contents lists available at ScienceDirect

Current Research in Pharmacology and Drug Discovery

journal homepage: www.journals.elsevier.com/current-research-in-pharmacology-and-drug-discovery

Inhalation potential of N-Acetylcysteine loaded PLGA nanoparticles for the management of tuberculosis: *In vitro* lung deposition and efficacy studies☆

Vishal Puri [a], Kabi Raj Chaudhary [a], Arti Singh [b], Charan Singh [a,*]

[a] Department of Pharmaceutics, ISF College of Pharmacy, GT Road NH-95, Ghal Kalan, Moga, Punjab, 142001, India
[b] Department of Pharmacology, ISF College of Pharmacy, GT Road NH-95, Ghal Kalan, Moga, Punjab, 142001, India

ARTICLE INFO

Keywords:
N-Acetylcysteine
PLGA
Pluronic F-127
Inhalation
Lung targeting
Tuberculosis

ABSTRACT

Several studies have stated that mucus is a critical hurdle for drug delivery to the mucosal tissues. As a result, Polymeric nanoparticles that can overcome mucus barriers are gaining popularity for controlled drug delivery into intra-macrophages to attain high intracellular drug concentration. The present study was aimed to fabricate inhalable N-acetylcysteine (NAC) modified PLGA mucus penetrating particles using the double emulsion method (w/o/w) for target delivery to alveolar macrophages and minimize the dose-related adverse effects, efficiently encapsulate hydrophilic drug, sustain the release profile and prolong the retention time for the management of tuberculosis. Among the numerous formulations, the drug/polymer ratio of 1:10 with 0.50% PVA concentration and sonication time for 2 min s was chosen for further research. The formulated nanoparticles had a mean particle size of 307.50 ± 9.54 nm, PDI was 0.136 ± 0.02, zeta potential about −11.3 ± 0.4 mV, decent entrapment efficiency (55.46 ± 2.40%), drug loading (9.05 ± 0.22%), and excellent flowability. FTIR confirmed that NAC and PLGA were compatible with each other. SEM graphs elucidated that the nanoparticles were spherically shaped with a slightly rough surface whereas TEM analysis ensured the nanometer size nanoparticles and coating of lipid over NPs surface. PXRD spectrum concluded the transformation of the drug from crystalline to amorphous state in the formulation. *In vitro* release pattern was biphasic started with burst release (64.67 ± 1.53% within 12hrs) followed by sustained release over 48hrs thus enabling the prolonged replenishing of NAC. *In vitro* lung deposition study pronounced that coated NAC-PLGA-MPPs showed favorable results in terms of emitted dose (86.67 ± 2.52%), MMAD value (2.57 ± 0.12 μm), GSD value (1.55 ± 0.11 μm), and FPF of 62.67 ± 2.08% for the deposition and targeting the lungs. Finally, *in vitro* efficacy studies demonstrated that NAC-PLGA-MPPs presented more prominent antibacterial activity against *MTB* H37Rv strain as compared to NAC. Hence, PLGA based particles could be a better strategy to deliver the NAC for lung targeting.

1. Introduction

Tuberculosis (TB) is a lethal communicable disease caused by bacillus *Mycobacterium tuberculosis (MTB),* which affects the human race by manifesting in the lungs predominately through the formation of soft tissue called granuloma (Singh et al., 2017).The World Health Organization (WHO) report of 2020 estimated 7.1 million newly diagnosed cases and 1.4 million deaths worldwide including 2,08,000 among HIV-positive patients (Organization WH, 2020; Chakaya et al., 2021). Even though WHO has recommended effective chemotherapy, TB remains a fatal disease due to poor patient compliance, induces oxidative stress, drug-induced toxicity, the complexity of treatment along with multidrug-resistant (MDR), and extensively drug-resistant (Dheda et al., 2017). These limitations draw the attention of researchers to develop an anti-TB drug delivery system with sustained release, low dosing frequency, targeted drug delivery, enhancing therapeutic efficacy, and reduced adverse effects (Nasiruddin et al., 2017).

N-acetyl-L-cysteine (NAC)is included in the list of essential medicines by WHO and approved by the Federal and Drug Administration (FDA) as an antidote for a hepatotoxic dose of acetaminophen (WHO, 2017; Prescott et al., 1979). NAC act as an antioxidant (stimulating the glutathione level), free radical scavenger, mucolytic agent, anti-inflammatory, and antimycobacterial effect by enhancing interleukins and interferon-gamma (INF-γ) production (Amaral et al., 2016; Yudhawati

☆ Affiliated to I. K. Gujral Punjab Technical University, formerly Punjab Technical University, Kapurthala, Jalandhar-Punjab 144,603, India.

* Corresponding author.
E-mail address: c.singhniper009@gmail.com (C. Singh).

https://doi.org/10.1016/j.crphar.2022.100084
Received 11 August 2021; Received in revised form 6 January 2022; Accepted 12 January 2022

and Prasanta, 2020). Furthermore, multiple clinical trials assured that NAC not only displayed synergistic, hepatoprotective, and otoprotective effects against anti-TB drugs but also emerged as an adjunct therapy in patients with neuropsychiatric disorders, cancer, and specifically for cardiovascular diseases (Naveed et al., 2017; Ejigu and Abay, 2020). Even though NAC belongs to BCS Class I i.e., high solubility and high permeability but common pitfall with NAC is a low bioavailability (~10%) which affects the drug therapeutic efficacy (Olsson et al., 1988). The major challenge which researchers encountered is the development of a carrier to stabilize the drug, target delivery, substantially improve the drug bioavailability and prevent premature degradation of proteins and peptides (Sharma et al., 2016). In such a scenario, drug encapsulation in polymeric nanoparticles and directly delivered to the lungs via inhalational route will be an ideal choice to improve the drug concentration at the local site of action (Parumasivam et al., 2016). Poly (lactic-co-glycolic acid)(PLGA) based inhalable powders have received a lot of attention in recent years (Emami et al., 2019). PLGA is US FDA (Food and Drug Administration) approved, biocompatible, biodegradable, and non-toxic polymer (Arpagaus, 2019). Additionally, it allows extended-release of encapsulated agents, possess surface decoration potential, and highly desirable in designing nano-sized particles (Tafaghodia et al., 2020). Mucus onto the surface of the lung presents a great challenge via inhalation delivery. Therefore, designing of mucus penetrating particles (MPP)by using Pluronic F127 could be a promising approach to overcome this barrier for better-targeted delivery and therapeutic efficacy. Meanwhile, the coating of NAC-loaded PLGA nanoparticles with Pluronic F127 greatly inhibits the adhesive interactions between PLGA core and mucus without modifying the PLGA carrier material.

Therefore with this motivation in mind, we developed and evaluated NAC-loaded PLGA nanoparticles coated with Pluronic F127 (NAC-PLGA-MPPs) for inhalation delivery. We prepared the nanoformulations using the double emulsion solvent evaporation (w/o/w) method and subjected to physicochemical characterization such as FTIR, DSC, FESEM, TEM, and PXRD. Additionally, we determined the *in vitro* release studies of NAC-PLGA-MPPs to examine the sustained release of NAC. Moreover, powder flow characterization and *in vitro* lung deposition studies were performed to assess the inhalation potential of these particles. Finally, *in vitro* efficacy studies were also performed using the BACTEC method.

2. Materials and methods

2.1. Materials

N-Acetyl-L-cysteine (NAC) and polyvinyl alcohol (PVA) were purchased from TCI Chemicals, India. Poly (d,l-lactide-co glycolide) (50:50) and Pluronic F127 were obtained from Sigma Aldrich, New Delhi, India while dichloromethane was provided by SRL Laboratory Pvt. Ltd., New Delhi, India. All other chemicals used were of analytical grade and used as supplied.

2.2. Methods

2.2.1. Synthesis of NAC loaded MPPs

The various formulations were designed to determine the effect of drug/polymer ratio, stabilizer, and coating material as indicated in Table 1.Initially, 10 mg of NAC was dissolved in 1 ml of distilled water ($water_{internal}$ phase) and emulsified with 3 ml dichloromethane (DCM) containing 50 mg, 100 mg, and 150 mg of PLGA (oil phase) and sonicated using a probe sonicator [SONICS VIBRA CELL (VCX 130 PB),USA] at different time interval about 1min, 2min and 3min to form the primary emulsion (w/o). The w/o emulsion was significantly emulsified with 5 ml PVA solution at varying concentrations of 0.25%/w/v, 0.5%w/v, and 0.75%w/v ($water_{external}$ phase) with continuous stirring followed by intermittent sonication to produce double emulsion(w/o/w). Furthermore, an equivalent volume of 2%v/v of Pluronic F127 was added to the formulation and 4 h of stirring will completely evaporate the organic solvent from the dispersed phase under reduced pressure. Finally, the emulsion was lyophilized at −30°C for 24hrs before being freeze-dried at 40°C for 48hrs (Christ Alpha 1–4 LOC-1M, Germany). In another formulation, the procedure was followed similarly as mentioned above except that Pluronic F127 was omitted from the formulation. Schematic representation of NAC-PLGA-MPPs is illustrated in Fig. 1.

2.3. Physicochemical characterization of nanoparticles

2.3.1. Particle size, PDI, and zeta potential

The particle size, polydispersity index, and zeta potential were determined by Dynamic Light Scattering using Delsa Nano C (Beckman Coulter Counter, USA). The glass cuvette was filled with a homogenized

Table 1
Composition and physical characterization of acetylcysteine loaded polymeric mucus penetrating particles.

Formulation	Drug/Polymer Ratio (w/w)	Water Added	Solvent (DCM)	PVA conc (% w/v)	Sonication time	Mean particle size (nm±SD)	PDI (±SD)	Zeta potential (mV±SD)	Entrapment efficiency (% EE±SD)	Drug loading (% DL ±SD)
F1	1:05	1 ml	3 ml	0.25	1min	312.53 ± 20.04	0.228 ± 0.06	−11.5 ± 1.5	35.10 ± 2.14	3.85 ± 0.35
F1	1:10	1 ml	3 ml	0.25	1min	252.93 ± 13.57	0.201 ± 0.06	−10.2 ± 0.6	37.85 ± 0.84	5.45 ± 0.08
F1	1:15	1 ml	3 ml	0.25	1min	272.47 ± 9.32	0.103 ± 0.07	−10.7 ± 1.4	34.41 ± 0.52	2.15 ± 0.03
F2	1:05	1 ml	3 ml	0.50	2min	350.47 ± 45.98	0.195 ± 0.10	−12.6 ± 1.9	54.18 ± 1.75	5.03 ± 0.29
F2	1:10	1 ml	3 ml	0.50	2min	307.50 ± 9.54	0.136 ± 0.02	−11.3 ± 0.4	55.46 ± 2.40	9.05 ± 0.22
F2	1:15	1 ml	3 ml	0.50	2min	345.57 ± 6.48	0.207 ± 0.06	−12.1 ± 1.8	46.88 ± 0.25	2.93 ± 0.01
F3	1:05	1 ml	3 ml	0.75	3min	640.37 ± 18.35	0.271 ± 0.02	−18.9 ± 1.2	29.86 ± 1.10	2.98 ± 0.18
F3	1:10	1 ml	3 ml	0.75	3min	725.23 ± 8.70	0.355 ± 0.03	−23.4 ± 1.7	32.07 ± 0.71	4.92 ± 0.06
F3	1:15	1 ml	3 ml	0.75	3min	815.40 ± 20.76	0.369 ± 0.01	−24.8 ± 2.3	30.41 ± 0.98	1.90 ± 0.06

The studies were performed in the triplicate (n = 3).

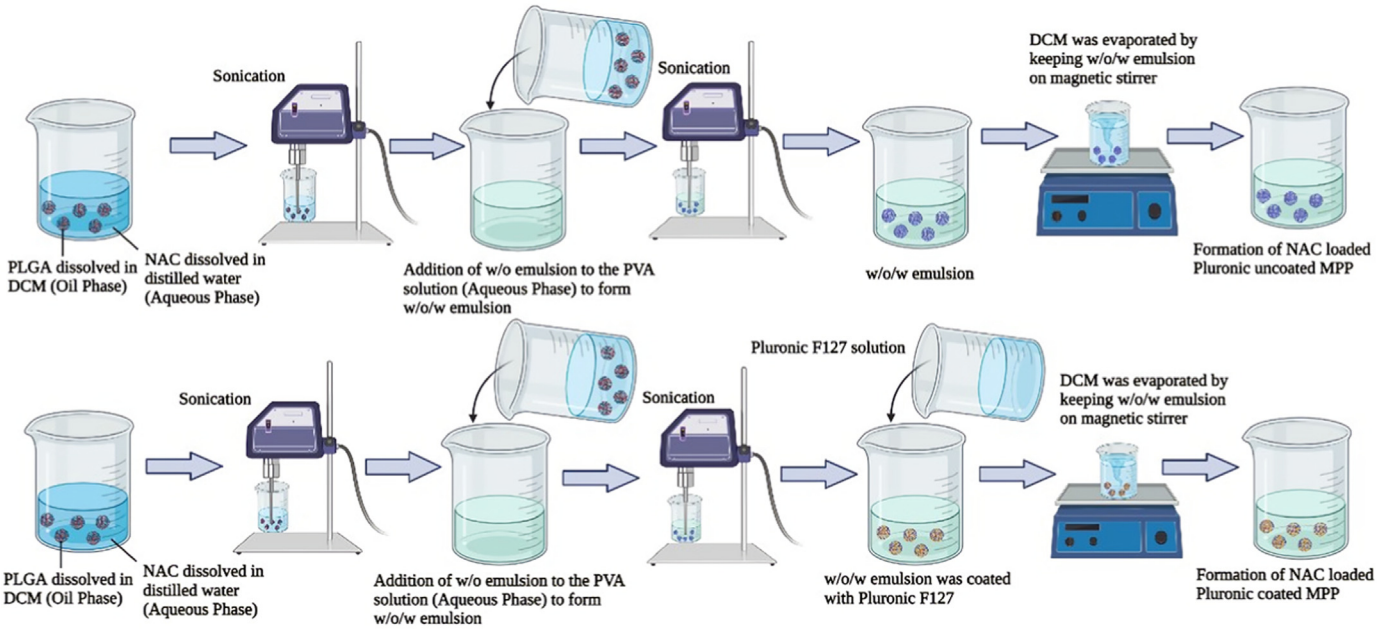

Fig. 1. Schematic representation of nanoparticles (A) without coated with Pluronic F127 (B) coated with Pluronic F127.

sample and then analyzed. All measurements were performed in triplicate (Bhattacharya et al., 2020).

2.3.2. Entrapment efficiency and drug loading

Entrapment efficiency (EE) and drug loading were estimated by the separation of free drug from the formulated nanoparticles using ultracentrifugation (indirect method). The suspension obtained after double emulsion was centrifuged at 4500rpm for 40min (Centrifuge 5418R Eppendorf, USA), and drug present in the supernatant was quantified by ultra violet spectrophotometer (UV-1700, Shimadzu, Japan) at 204 nm. Encapsulation efficiency was measured from the fraction of NAC encapsulated into NPs to the total amount of NAC initially added while the drug loading was described as the percentage of amount of NAC divided by total weight of mixture i.e., NAC and PLGA (Ahmaditabar et al., 2017; Abdelghany et al., 2019). The percent of entrapment efficiency and drug loading was calculated by using the following formula:

$$\%\ \text{Entrapment Efficiency} = \frac{\text{Total drug added} - \text{Amount of free drug}}{\text{Total drug added}} \text{x } 100 \quad (1)$$

$$\text{Drug Loading } (\mu g/mg) = \frac{\text{Amount of drug added} - \text{Unentrapped drug}}{\text{Weight of nanoparticles recovered}} \text{x } 100 \quad (2)$$

2.3.3. Fourier transforms infrared spectroscopy (FT-IR)

The infrared spectrum provides extensive information about the functional group present in a formulation. It is mostly used to examine the chemical interaction between drugs and excipients. FT-IR spectra of NAC, PLGA, physical mixture of NAC, PLGA plus Pluronic F127, and NAC-PLGA-MPPs were detected by FT-IR spectrometer (Agilent Cary 630, USA) using KBr disk method were sample (2 mg each) were mixed with potassium bromide and transformed into the pellet. The spectra were analyzed in the wavelength range of 400-4000 cm^{-1} (Budama-Kilinc et al., 2018).

2.3.4. Differential scanning calorimetry (DSC)

DSC monitors the temperature and heat flow associated with thermal transitions in a material so that the amorphous and crystalline behavior of the drug in nanoparticles could be identified. DSC curves of pure drug, polymer, physical mixture, and resulting nanoparticles were measured by DSC 6000, PerkinElmer, USA. The instrument was calibrated with indium (99.9% pure calibration standard) and the melting point was recorded by heating 5 mg of each sample in an aluminum pan from 30 °C to 300 °C at a heating rate of 10 °C/min under a constant flow of nitrogen at 20 ml/min and cooling back to 30 °C at the same rate. An empty aluminum pan was taken as a reference (Zakeri-Milani et al., 2013).

2.3.5. Scanning electron microscopy (SEM)

SEM imaging was necessary to visualize the diameter, structural and surface morphology of the NAC-PLGA-MPPs. The powder was sprinkled into double-adhesive carbon tape that adhered to an aluminum stub, sputter-coated with a thin layer of gold, and analyzed (JEOL JSM-7610F Plus, Japan) with a 15 kV accelerating voltage at different magnifications (Khatak et al., 2020).

2.3.6. Transmission electron microscopy (TEM)

The surface coating and morphological characterization of coated and uncoated NAC-PLGA-MPPs were analyzed by TEM (Hitachi H-7500, Japan). A drop of nanoparticle dispersion was kept on the carbon-coated copper grid and stained with phosphotungstic acid (2% w/v) then air-dried and visualized under the TEM microscope with an accelerating voltage of 120 kV at various magnifications (Singh et al., 2015a).

2.3.7. X-ray diffraction study

The X-ray diffraction (XRD) analysis is performed to get the information regarding crystal lattice arrangement and identification of physical state i.e., crystalline and amorphous state of the drug in the formulation. The crystalline behavior of NAC, PLGA, NAC-PLGA-F127, and NAC-PLGA-MPPs was examined by powder X-ray diffraction (PXRD) (Bruker D8 Advance, Germany) by placing a sample on a horizontal quartz glass holder plate and using Cu K_α radiation (45 kV, 40 mA) with 2θ scan range of4 to 50° at a rate of 10°/min at 25 °C in a uniform scan mode (Singh et al., 2014).

2.3.8. In vitro drug release study

In vitro release profile was carried out by placing 20 mg NAC and NAC-PLGA-MPPs in a USP Dissolution Apparatus-II (Paddle type)

(DS8000, Lab India). The dissolution media consist of a 900 ml phosphate buffer solution (pH-7.4) with temperature maintained at 37 ± 0.5 °C and a paddle rotating at 50rpm. Precisely, 5 ml of suspension was withdrawn at predetermined time intervals (1 h, 2hrs, 4hrs, 6hrs, 8hrs, 10hrs, 12hrs, 24hrs, and 48hrs) and replaced with 5 ml of buffer solution to maintain the sink condition. The drug content was detected by a UV spectrophotometer (UV-1700 Shimadzu, Japan) at 204 nm (Khaira et al., 2014).

2.3.9. Bulk and tapped density

The initial and final volume (after tapping) was noted for the computation of bulk and tapped density. Owing to the sample size constraint, a precisely weighed powder (1g) was filled into a 10 ml graduated cylinder and operated for a fixed number of taps (200) (Bosquillon et al., 2001). The compressibility index of the powder was calculated using the following equation based on the apparent bulk and tapped density.

$$Carr's\ index = \frac{\text{Tapped density} - \text{Bulk density}}{\text{Tapped density}} \text{x } 100 \quad (3)$$

2.3.10. Powder flowability

The flow properties of the lyophilized powder were performed by an angle of repose and Hausner ratio because these are convenient and simple method adapted for semi-cohesive powders. The angle of repose was measured using the fixed funnel technique, where the powder is poured into a flat horizontal surface through a funnel to form a conical pile with an angle Θ (Ezzati Nazhad Dolatabadi et al., 2015). The value of Θ was calculated by inverting the height to the sloping surface of the pile. The Hausner ratio was obtained by dividing the tapped density by the bulk density.

$$\theta = \tan^{-1}(h/r) \quad (4)$$

Where, h = height, r = radius

$$Hausnerr\ ratio = \frac{\text{Tapped density}}{\text{Bulk density}} \quad (5)$$

2.3.11. In vitro pulmonary deposition studies

The aerodynamic evaluation of uncoated and coated NAC-PLGA-MPPs was carried out using a next-generation cascade impactor (NGI)(-Copley Scientific Limited, Nottingham, UK)equipped with a USP induction port (Apparatus 1, USP 35) where the powder was aerosolized at a flow rate of 30L/min and measured by a flow meter (DFM2, Copley Scientific, UK). Before the dispersion, all NGI stages were coated with 1.5%w/v of hydroxypropyl methylcellulose (HPMC) (4000cps) gel in water to reduce the particle bouncing. The HPMC hard gelatin capsules (size 3, Quali-V®, Qualicaps® Inc, Whitsett, USA) were loaded with 20 mg of powder per capsule followed by actuation for 10sec using an Osmohaler® (Plastiape, Italy). Powder deposited at each NGI stage was extracted, rinsed with methanol, and centrifuged for 15 min at 5000 rpm(Centrifuge 5418R Eppendorf, USA), the supernatant was collected and subjected to HPLC analysis. Aerodynamic parameters including emitted dose (ED), fine particle fraction (FPF), mass median aerodynamic diameter (MMAD), and geometric standard deviation (GSD) were calculated (Lababidi et al., 2020; Singh et al., 2015b) as follows:

$$\text{Emitted dose (ED\%)} = \frac{\text{Initial mass in capsules} - \text{Final mass remaining in capsules}}{\text{Initial mass in capsules}} \text{x } 100 \quad (6)$$

$$\text{Fine particle fraction (FPF\%)} = \frac{\text{Mass deposited}}{\text{Initial particle mass loaded in capsules}} \text{x } 100 \quad (7)$$

2.3.12. In vitro antimycobacterial activity

The minimum inhibitory concentration (MIC) and minimum bacterial concentration (MBC) of NAC and NAC-PLGA-MPPs against *MTB* H37Rv strain (Tuberculosis Research Centre, Chennai, India) were examined using BACTEC method (Venkataraman et al., 1998).The bacteria were cultured in Middlebrook 7H9 broth supplemented with 10% oleic acid-albumin- dextrose-catalase (OADC; HiMedia, India) and stored in aliquots at −60 °C until required. The sample was dissolved in distilled water and sterilized with Middlebrook 7H9 before testing. The MTB growth index (GI) was determined by BACTEC™ MGIT™ 960 System(-FIND Diagnostics, USA). Briefly, 0.1 ml was added to BACTEC 12B vials and incubated at 37 °C in a CO_2enriched atmosphere. After incubation, MIC was recorded as the lowest concentration of the NAC that completely suppress the growth. The GI value was analyzed daily under anaerobic conditions in 1:100 control until a value greater than 30 was obtained. Moreover, undiluted control reading was used to assess the percentage inhibition (Singh et al., 2015b). Both positive and negative controls consisting of either bacterial suspension or broth alone were included in all test groups. The percentage of growth inhibition was estimated for each drug concentration. MBC of NAC was defined as the lowest concentration of the agent that caused ≥99.9% killing of the inoculum.

3. Results

3.1. Particle size, PDI, and zeta potential analysis

Table 1 depicted the various physical parameters of the NAC-PLGA-MPPs where nano-sized particles were obtained along with monodisperse size distribution. The smallest particle size (252.93 ± 13.57 nm), PDI value (0.201 ± 0.06), and zeta potential (−10.2 ± 0.6 mV) were observed in the F1 formulation containing 0.25% PVA and 1:10 drug/polymer ratio. Although the mean particle size (307.50 ± 9.54 nm) and negative zeta potential (−11.3 ± 0.4 mV) of F2 formulation containing 0.50% PVA with 1:10 drug/ polymer ratio was similar to the F1 value whereas other characteristics such as PDI (0.136 ± 0.02), entrapment efficiency, and drug loading of F2 formulation were more promising. After coating with Pluronic F127, particle size obtained was 382.63 ± 6.42 nm, PDI of 0.208 ± 0.01, and zeta potential about-14.3 ± 2.1 mV. On this basis, F2 was a preferred formulation for developing NAC-PLGA-MPPs.

3.2. Entrapment efficiency and drug loading

Entrapment efficiency and drug loading are considered integral parameters from the perspective of formulation and large-scale manufacturing. The lowest EE (29.86 ± 1.10) and DL (1.90 ± 0.06) were observed in F3 formulation with drug/polymer ratio varies from 1:05 to 1:15. On the other hand, optimized formulation F2 showed maximum EE (55.46 ± 2.40%) and DL (9.05 ± 0.22%) of NAC as shown in Table 1.

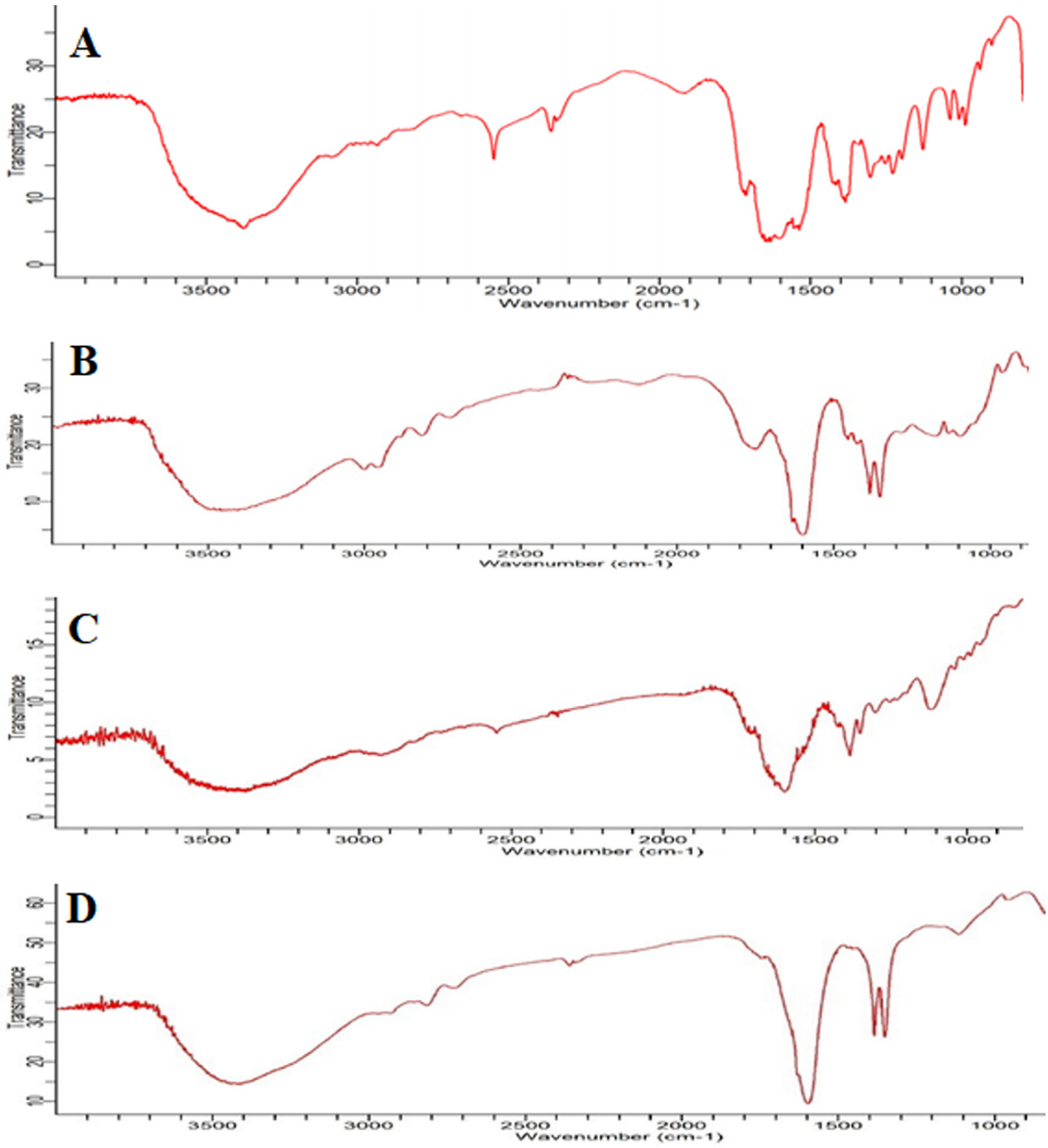

Fig. 2. Fourier transform infrared (FTIR) spectrum of (A) pure NAC (B) PLGA (C) physical mixture of NAC-PLGA-F127 and (D) NAC-PLGA-MPPs.

3.3. Fourier transform infrared spectroscopy (FT-IR)

The schematic representation of the FT-IR spectrum is mentioned in Fig. 2 and functional groups present at different vibrational frequencies are described in Table 2. In the NAC spectra, the distinctive peak at 2549 cm^{-1} due to SH stretching and 3372 cm^{-1}indicative of N–H band (Fig. 2A) while 1715 cm^{-1} owing to stretching of C═O carboxylic group confirm the presence of PLGA (Fig. 2B) (Guerini et al., 2020). In addition, 1184 cm^{-1} attributed to the C–N group, 1535 cm^{-1} assigned to N–H stretching vibrations of NH group, and CH_3group present at 1450 cm^{-1}. The disappearance of the S–H peak in the NAC-PLGA-MPPs exhibited the excellent bonding between the sulfhydryl group of NAC and the surface of the formulation thus evidence of successful drug loading (Du et al., 2017). The amide I, II, and III was ascribed at 1560, 1530, and 1275-1370 cm^{-1} respectively. Moreover, NAC-PLGA-MPPs exhibited the additional peaks of amide I, II, carboxylic, S–H group, and a low-intensity band of NH hereby confirming the NAC presence in nanoparticles (Fig. 2D). Meanwhile, the band in PLGA and physical mixture at 2996 cm^{-1} consist of alkyl groups, 1751 cm^{-1} of carbonyl stretching group whereas 1100-1176 cm^{-1} comprises of the ester group (mainly C–O band) which linked with water and undergoes PLGA hydrolysis hereby ensuring a sustained release of NAC from nanoparticles (Fig. 2C) (Makadia and Siegel, 2011). There were no prominent changes in the PLGA and NAC-PLGA-MPPs spectra which suggested the remarkable stability of polymer in the nanoparticles. In the physical mixture, Pluronic F127 presence is attributed by the characteristic peaks at 1345 cm^{-1}, 1298 cm^{-1}, 1249 cm^{-1}, and 952 cm^{-1} which are related to CH_2 stretching vibration (Lin et al., 2009). The crystallinity of the PVA was identified at 1120 cm^{-1} which was related to the C–O stretching band (Fig. 2D) (Mansur et al., 2008).

Table 2
FT-IR functional groups present at various vibrational frequencies (Wave numbers/cm^{-1}).

Formulation	Frequencies	Functional Group
NAC (Drug)	2549 cm^{-1}	SH stretching
	3372 cm^{-1}	N–H band
	1184 cm^{-1}	C–N stretching
	1535 cm^{-1}	N–H stretching vibrations of NH group
	1450 cm^{-1}.	CH_3 group
PLGA (Polymer)	1715 cm^{-1}	C=O carboxylic group
	2996 cm^{-1}	Alkyl groups
	1751 cm^{-1}	Carbonyl stretching group
	1100-1176 cm^{-1}	Ester group
NAC-PLGA-F127 (Physical Mixture)	2996 cm^{-1}	Alkyl groups
	1751 cm^{-1}	Carbonyl stretching group
	1100-1176 cm^{-1}	Ester group
	1345 cm^{-1}, 1298 cm^{-1}, 1249 cm^{-1}, and 952 cm^{-1}	CH_2 stretching vibration
NAC-PLGA-MPPs (Formulation)	1560 cm^{-1}	Amide I
	1530 cm^{-1}	Amide II
	1275-1370 cm^{-1}	Amide III
	1535 cm^{-1}	N–H stretching vibrations of NH group
	1120 cm^{-1}	C–O stretching band

3.4. Differential scanning calorimetry (DSC)

The DSC thermogram depicted a glass transition for PLGA at ~60 °C (Fig. 3B). The melting point of NAC was desirable at ~110 °C while the steep peak indicated that the drug was in a crystalline form as observed in pure drug and the physical mixture (Fig. 3A and C). In the physical mixture, the melting temperature (T_m) of the polymer was 50 °C and 102 °C for NAC whereas the melting point for Pluronic F127 in the formulation was reported at 45 °C.Besides this, there was a small endothermic peak at 220–230 °C which corresponds to the phase transition of PVA. Surprisingly, the broadening peak of the PLGA polymer and disappearance of melting peaks instead of the intense sharp peak of the drug in the NAC-PLGA-MPPs further scrutinized that NAC was integrated into the polymer matrix; thus exists in the amorphous or partially crystalline state (Fig. 3D) (Mahumane et al., 2020). This study also iterates the presence of the drug in a solubilized state in the lipid due to solid-state interaction induced by heating as mentioned in Fig. 3.

3.5. Scanning electron microscopy (SEM)

The SEM images of NAC-PLGA-MPPs were demonstrated in Fig. 4. The nanoparticles were discovered to be spherical with a smooth surface. A narrow size range (<500 nm) was visualized which is favorable for internalization into alveolar macrophages (Fig. 4B) (Zarchi et al., 2015).

3.6. Transmission electron microscopy (TEM)

TEM analysis of NAC-PLGA-MPPs observed discrete and spherical-shaped particles with a dense coating over particle surface as highlighted in Fig. 5. TEM images anticipated that particle size was in nanometer range before and after coating with Pluronic F127; hence compatible for inhalation and easily phagocytosis by macrophages (Sanches et al., 2020).

3.7. X-ray diffractometry

The X-ray diffraction spectra of pure NAC, PLGA, physical mixture (NAC-PLGA-F127), and lyophilized NAC-PLGA-MPPs are shown in Fig. 6. NAC displayed multiple notable peaks but a high-intensity peak was obtained at a 2θ value of 27° on diffraction spectrum reflected the drug's crystallinity in its pure form (Fig. 6A). Interestingly, all of the NAC characteristic peaks in the physical mixture were obtained at the same position but with lower intensity (Fig. 6C) whereas PLGA was present in the amorphous form (Fig. 6B). Moreover, drug characteristic peaks were not present at a higher percentage in NAC-PLGA-MPPs suggesting that drug encapsulated in MPPs were amorphous or partially crystalline (Fig. 6D) (Desai et al., 2008).

3.8. In vitro release pattern

The release profile from NAC-PLGA-MPPs predicted a biphasic release that began with a burst release (64.67 ± 1.53% within 12hrs) followed by a sustained release of about 76.33 ± 0.57% in 48hrs as revealed in Fig. 7. Moreover, 100% of pure NAC was released abruptly within 2 min s (Chiesa et al., 2017). The burst release phase is characterized by swiftly drug release due to drug dissolution on the nanoparticles surface or initial exposure of PLGA nanoparticles to the aqueous environment which causes polymer erosion both within the bulk and at the particle surface, resulting in drug diffusion through aqueous pores whereas extended-release was due to strong interaction of NAC with the hydrophobic PLGA which impeded the release by integrating the drug into the matrix (Yoo and Won, 2020).

3.9. Powder characterization

The bulk density of lyophilized uncoated and coated NAC-PLGA-MPPs were 0.194 ± 0.015 and 0.178 ± 0.003 g/cm^3, respectively whereas the tapped density was 0.241 ± 0.019 g/cm^3 for uncoated and 0.192 ± 0.006 g/cm^3 for coated NAC-PLGA-MPPs as described in Table 3. Powder flow properties were calculated by carr's index, angle of repose, and Hausner ratio. The carr's index value of less than 15% proclaimed good flowability while greater than 25% pronounced cohesive flowing powder. The carr's index value varied from 7.08 ± 1.38% for coated (excellent flowability) to 19.5 ± 0.58% for uncoated formulation (fair flowability). The powder flowability is inversely related to the angle of repose, with a large angle of repose value suggesting poor flow characteristics and a small angle of repose indicating free-flowing powder (Mahajan and Gundare, 2014). The results highlighted a good angle of repose value for coated formulation (32.3 ± 2.08) and fair flowing property for uncoated NAC-PLGA-MPPs (37.7 ± 1.53). Hausner ratio of the lyophilized formulation was excellent about 1.07 ± 0.02 and for uncoated was found to be 1.24 ± 0.01 (Table 3). The findings elucidated that the proposed formulation has the potential for pulmonary drug delivery.

3.9.1. In vitro deposition study

The aerodynamic behavior of coated and uncoated NAC-PLGA-MPPs indicated the particles deposition on each stage of NGI (highest in stage-3) therefore can effectively disseminate throughout the lungs as scrutinized in Fig. 8. The aerodynamic particle size of 1–5 μm assured the target delivery to the alveolar region (Lee et al., 2015). Both formulations emitted >80% of dose thus exhibiting that maximum drug was available for the inhalation. The MMAD value for uncoated NAC-PLGA-MPPs was 2.35 ± 0.17 μm and for coated NAC-PLGA-MPPs was 2.57 ± 0.12 μm hence emerged to be sufficiently deposited in the lungs. Consequently, respirable FPF value was 55.33 ± 3.51% for uncoated and 62.67 ± 2.08% for coated NAC-PLGA-MPPs while GSD value for uncoated and coated nanoparticles was 1.47 ± 0.14 μm and 1.55 ± 0.11 μm, respectively (Sharma et al., 2020). The findings elucidated that the proposed formulation has the potential for pulmonary drug deliver (See Table 4).

3.10. In vitro antimycobacterial activity

To establish the *in vivo* potential of NAC and NAC-PLGA-MPPs, developed formulation was analyzed for antimycobacterial activity. The findings suggested that MIC value were found out to be 2.37 mg/ml and 0.64 mg/ml, respectively whereas MBC value was visualized to be

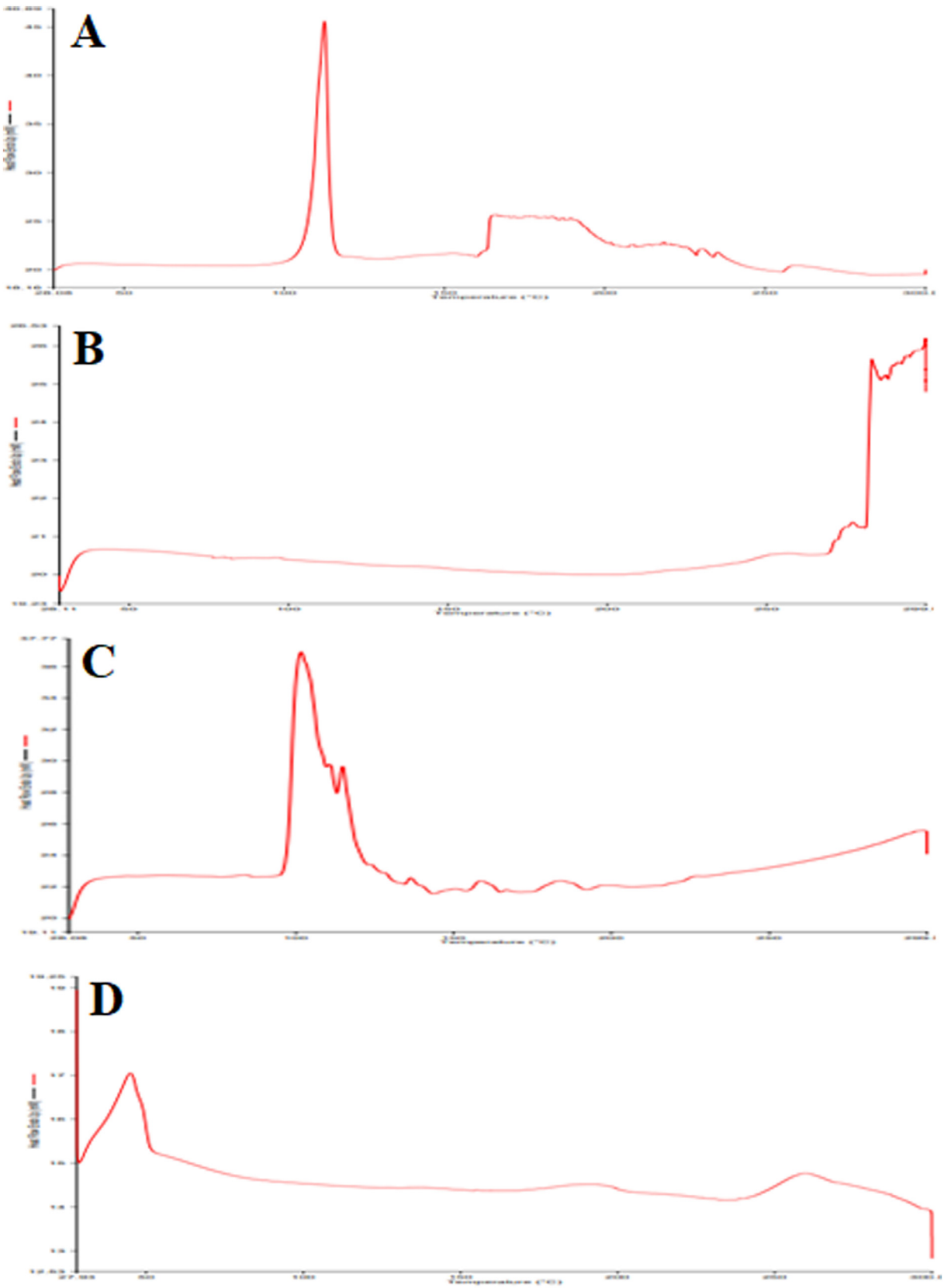

Fig. 3. Differential scanning calorimetric (DSC) thermograms of (A) NAC (B) PLGA (C) NAC-PLGA-F127 and (D) NAC-PLGA-MPPs.

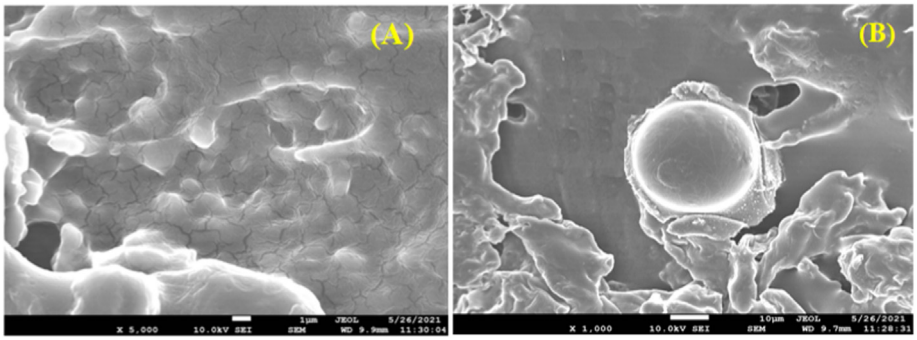

Fig. 4. Scanning electron micrographs (SEM) images of (A) Uncoated NAC-PLGA-MPPS and (B) Coated NAC-PLGA-MPPs.

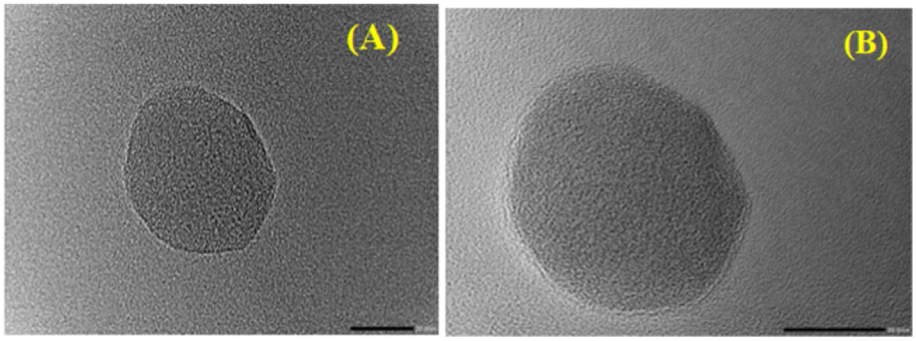

Fig. 5. Transmission electron microphotograph (TEM) of (A) Uncoated NAC-PLGA-MPPS and (B) Coated NAC-PLGA-MPPs.

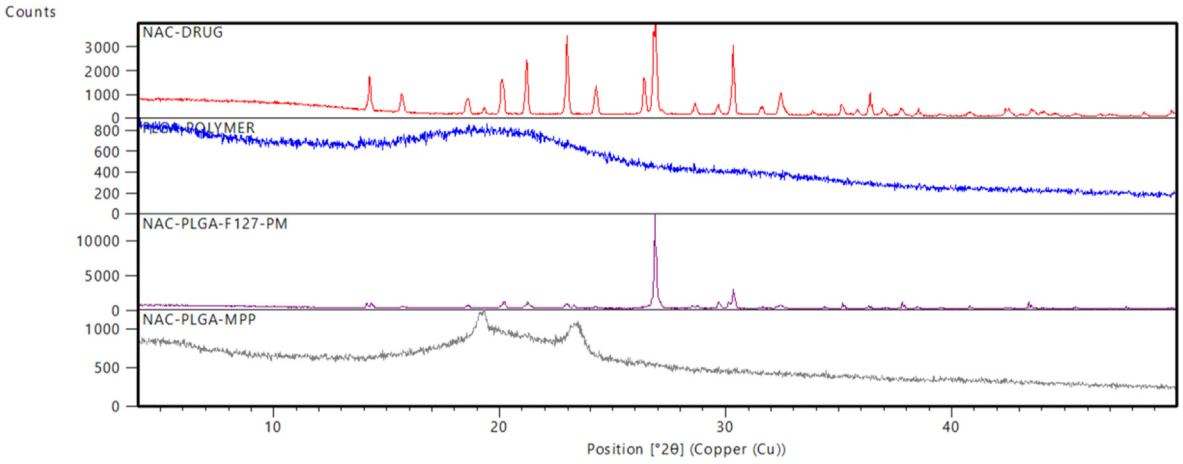

Fig. 6. X-ray diffraction data of (A) NAC (B) PLGA (C) NAC-PLGA-F127 (D) NAC-PLGA-MPPs. PM stands for the physical mixture.

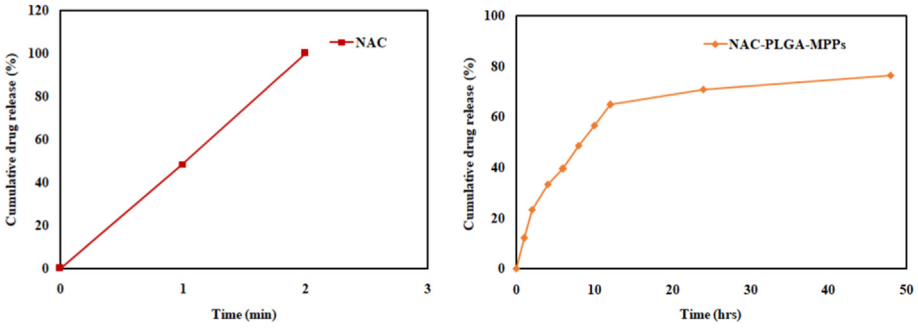

Fig. 7. Comparative *in vitro* release pattern of NAC and optimized NAC-PLGA-MPPs (n = 3).

Table 3
Powder flow characterization with and without Pluronic F127.

Formulation	Bulk density (g/cm^3)	Tapped density (g/cm^3)	Carr's index (%)	Angle of repose (Θ)	Hausner ratio
Uncoated NAC-PLGA-MPPs	0.194 ± 0.015	0.241 ± 0.019	19.5 ± 0.58	37.7 ± 1.53	1.24 ± 0.01
Coated NAC-PLGA-MPPs	0.178 ± 0.003	0.192 ± 0.006	7.08 ± 1.38	32.3 ± 2.08	1.07 ± 0.02

All measurements were performed in triplicate and standard deviation was calculated.

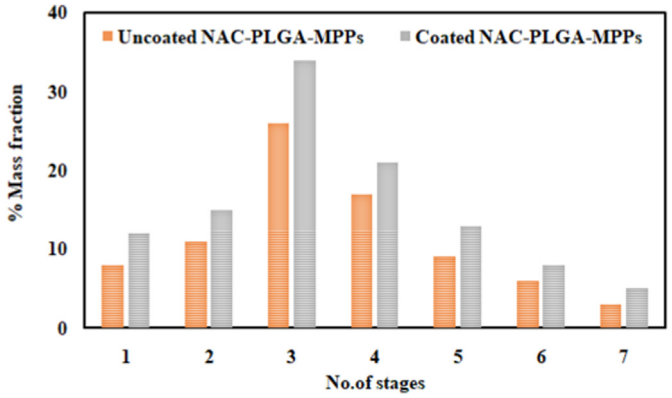

Fig. 8. *In vitro* aerosol deposition profile of uncoated and coated NAC-PLGA-MPPs on each stage following next-generation impactor (NGI) (mean ± SD, n = 3).

Table 4
Flowability scale.[a].

Flow character	Angle of repose	Carr's index	Hausner ratio
Excellent	25–30	<10	1.00–1.11
Good	31–35	11–15	1.12–1.18
Fair	36–40	16–20	1.19–1.25
Passable	41–45	21–25	1.26–1.34
Poor	46–55	31–36	1.35–1.45
Very poor	56–65	32–37	1.46–1.59
Very very poor	>66	>38	>1.60

[a] Data was taken from reference 45.

19.25 mg/ml for NAC and 5.18 mg/ml for the formulation (Zhao and Liu, 2010). NAC-PLGA-MPPs reported four-folds improved *in vitro* efficacy as compared to pure drug hence act as a bactericidal and completely inhibiting the *MTB* growth.

4. Discussion

Tuberculosis is a fatal infectious disease and is prevalent in least developed and developing countries (Singh et al., 2015c). The current regimen is long term and cumbersome which requires at least 6–9 months. In this research, NAC-PLGA-MPPs were designed to reduce the treatment time of the standard TB therapy from 6 to 9 months to possibly 1–2 months, as well as to achieve good encapsulation efficiency along with controlled and targeted drug delivery through pulmonary delivery. Moreover, it also envisions overcoming the biological barriers such as mucus and granuloma that developed during TB pathogenesis and are responsible for poor drug penetration. Mucus mesh-like network traps overseas particles via steric obstruction and adhesion through hydrophobic, electrostatic, hydrogen bonding interactions, van der Waals forces, and chain entanglement; hence eliminating particles in a quick interval time. For respiratory mucus penetration, nanoparticles ought to be of smaller size to prohibit steric obstruction and must be hydrophilic with a neutral surface to enhance mucoadhesion. When inhaled, NAC mucolytic activity is mediated by its free sulfhydryl group, which reduces the disulfide bonds in the mucus matrix and lowers the mucus viscosity. The double emulsion solvent evaporation (w/o/w) is the acceptable technique available for encapsulating hydrophilic drugs such as NAC (Iqbal et al., 2015). While incorporating the drug into polymeric nanoparticles has the advantage of being readily internalized into alveolar macrophages with optimum particle size range and aerodynamic diameter. This could results in improved antimycobacterial activity to limit the *MTB* infection through suppression of host oxidative response and disrupt *MTB* biofilm formation. In this work, nine batches of nanoparticles were synthesized and optimization was done to examine the effect of process parameters primarily sonication time and formulation parameters such as drug: polymer ratio, polymer, and polyvinyl concentration on the particle size. The results predicted that increasing the PVA concentration would decrease the particle size nevertheless increasing the polymer concentration eventually increased the particle size. Initially, increasing the drug: polymer ratio results in enhanced entrapment efficiency and drug loading. Soon after, both EE and DL were decreased which might be attributed to the polymer's separation tendency (Tripathi et al., 2010). The lower EE and DL value was probably due to NAC hydrophilic nature which leaches out the drug to the outer aqueous phase (Chen and Wen, 2018). Desai et al. synthesized PLGA implants with 1–10% w/w of NAC using solvent extrusion and fluid energy micronization (FEM) method. They reported the DL in the range 0.96–8.5% and EE of 82–95% (Desai et al., 2008). Similarly, Zarchi et al. declared that NAC incorporated PLGA nanoparticles when fabricated by electrospray technique, had DL about 5% and EE was 54.5% (Zarchi et al., 2015). In the literature, there were several modifications performed to enhance the EE (85–95%) and DL value (~10%) which is desirable for large-scale commercial manufacturing (Chong et al., 2015; Khadem-Hamedani, 2019; Winkler et al., 2019).

Besides this, the sonication time was optimized to provide a stable formulation with appropriate particle size and % drug entrapment. Moreover, droplet size was not affected by the nonsolvent viscosity, type of solvent, or the amount of drug used. The outcomes concluded that a desirable formulation was obtained after sonicating for 2 min in a pulsed manner. However, augmenting the sonication time (3 min) resulted in larger particle size (640–815 nm) along with lower drug entrapment (29–32%) and drug loading (1–4%) due to particle agglomeration caused by surface charge. FT-IR spectrum of physical mixture concluded no distinctive changes compared to the formulation. DSC thermograms and PXRD analysis ensured the decreased crystallinity and absence of distinctive peaks in the formulation which proved the amorphization or drug solvation in the amorphous carrier. SEM and TEM results declared nano-sized spherical particles. In the *in vitro* release studies, the rapid initial drug release was attributed to the fact that NAC was absorbed at nanoparticle surface or large surface to volume ratio of nanoparticle geometry because of their size or due to water-soluble nature of NAC whereas diffusion of the dissolved drug within the PLGA core into the dissolution medium was responsible for the delayed-release pattern. Similar findings were claimed by other researchers working on NAC-PLGA nanoparticles (Chiesa et al., 2018). Powder characterization results revealed that the formulation had improved aerosolization which is linked with reduced powder density (Labiris and Dolovich, 2003). *In vitro*

Table 5
Aerodynamic characterization of uncoated and coated NAC-PLGA-MPPs.

Formulation	ED (%)	MMAD (μm)	GSD (μm)	FPF (%)
Uncoated NAC-PLGA-MPPs	83.33 ± 1.53	2.35 ± 0.17	1.47 ± 0.14	55.33 ± 3.51
Coated NAC-PLGA-MPPs	86.67 ± 2.52	2.57 ± 0.12	1.55 ± 0.11	62.67 ± 2.08

All results were accomplished in triplicates under constant conditions (n = 3).

deposition study scrutinized that coated NAC-PLGA-MPPs displayed superior aerosol powder performance thereby suitable for administration in the form of dry powder inhalation (DPI) for deep deposition in the lungs as illustrated in Table 5. Drug loaded PLGA MPPs exhibited enhanced *in vitro* antimycobacterial activity against $H_{37}Rv$ strain**.** This could be attributed to reduced particle size and better uptake of the nanoparticles vis-à-vis unformulated drug. Finally, the outcomes of the current work suggested that NAC-PLGA-MPPs can be an effective "adjunct therapy" in tuberculosis treatment but clinical trials on a potent drug-like N-acetylcysteine are obligated to not only decline the TB incidence but to eradicate this lethal disease globally to the level where TB is regarded as a disease of the past.

5. Conclusions

This paper focuses on the development of a new formulation of NAC containing PLGA nanoparticles using double emulsion method to reduce the NAC dose compared to oral route of administration and enhancing the efficacy via deep lung delivery at the local site of action. In this work, the developed formulation showed a desired particle size for deep lung delivery and sustained release (76.33 ± 0.57%) up to 48hrs. Additionally, the powder flow properties displayed good flowability of NAC-PLGA-MPPs; which shows PLGA nanoparticles an ideal delivery system for mucus penetration to reach the lungs deeply with increased retention for the management of TB. Moreover, the physicochemical properties of nanoparticles may be altered by modifying the parameters such as drug/polymer ratio, aqueous phase volume, and sonication time. Finally, for the clinical translation of the developed formulation cell based assays and mucus penetration potential could be assessed in future. In addition to this, the ultimate proof of lung deposition can be confirmed only after the *in vivo* aerosolization experiments carried out in animal model. In a nutshell, it can be concluded that mucus penetrating particles open the doorstep for researchers to investigate the inhalational delivery of NAC which has the potential to be employed in various biomedical applications.

CRediT authorship contribution statement

Vishal Puri: Performed the experimental work and written the manuscript. **Kabi Raj Chaudhary:** Contributed in the powder flow properties and in vitro release studies. **Arti Singh:** Critically examined the manuscript. **Charan Singh:** Conceptualized the research work and edited the manuscript.

Declaration of competing interest

The authors declare that they have no known competing financial interests or personal relationships that could have appeared to influence the work reported in this paper.

Acknowledgments

Authors are grateful to ISF College of Pharmacy, Moga, Punjab. The authors also would like to acknowledge CIF, LPU, SAIF, and CIL facility, PU for sample analysis support.

References

Abdelghany, S., Parumasivam, T., Pang, A., Roediger, B., Tang, P., Jahn, K., Britton, W.J., Chan, H.K., 2019. Alginate modified-PLGA nanoparticles entrapping amikacin and moxifloxacin as a novel host-directed therapy for multidrug-resistant tuberculosis. J. Drug Deliv. Sci. Technol. 52 (1), 642–651.

Ahmaditabar, P., Momtazi-Borojeni, A.A., Rezayan, A.H., Mahmoodi, M., Sahebkar, A., Mellat, M., 2017. Enhanced entrapment and improved *in vitro* controlled release of n-acetyl cysteine in hybrid PLGA/lecithin nanoparticles prepared using a nanoprecipitation/self-assembly method. J. Cell. Biochem. 118 (12), 4203–4209.

Amaral, E.P., Conceição, E.L., Costa, D.L., Rocha, M.S., Marinho, J.M., Cordeiro-Santos, M., D'Império-Lima, M.R., Barbosa, T., Sher, A., Andrade, B.B., 2016. N-acetyl-cysteine exhibits potent anti-mycobacterial activity in addition to its known anti-oxidative functions. BMC Microbiol. 16 (1), 1, 0.

Arpagaus, C., 2019. PLA/PLGA nanoparticles prepared by nanospray drying. J. Pharm. Invest. 49 (4), 405–426.

Bhattacharya, S., Puri, V., Sharma, S., Sahoo, D., Pal, P.K., Kujur, S., Goyal, G., Singh, A., 2020. Preparation and evaluation of sodium alginate microparticles using pepsin. J. Drug Deliv. Therapeut. 15 (2), 5–11, 10.

Bosquillon, C., Lombry, C., Preat, V., Vanbever, R., 2001. Influence of formulation excipients and physical characteristics of inhalation dry powders on their aerosolization performance. J. Contr. Release 70 (3), 329–339, 23.

Budama-Kilinc, Y., Cakir-Koc, R., Kecel-Gunduz, S., Kokcu, Y., Bicak, B., Mutlu, H., Ozel, A.E., 2018. Novel NAC-loaded poly (lactide-co-glycolide acid) nanoparticles for cataract treatment: preparation, characterization, evaluation of the structure, cytotoxicity, and molecular docking studies. PeerJ 30 (6), e4270.

Chakaya, J., Khan, M., Ntoumi, F., Aklillu, E., Razia, F., Mwaba, P., Kapata, N., Mfinanga, S., Hasnain, S.E., Katoto, P.D., Bulabula, A.N., 2021. Global tuberculosis report 2020–reflections on the global TB burden, treatment, and prevention efforts. Int. J. Infect. Dis. 11.

Chen, G., Wen, J., 2018. Poly (lactic-co-glycolic acid) based double emulsion nanoparticle as a carrier system to deliver glutathione sublingually. J. Biomed. 3, 50–59.

Chiesa, E., Monti, L., Paganini, C., Dorati, R., Conti, B., Modena, T., Rossi, A., Genta, I., 2017. Polyethylene glycol-poly-lactide-co-glycolide block copolymer-based nanoparticles as a potential tool for off-label use of N-acetylcysteine in the treatment of diastrophic dysplasia. J. Pharmaceut. Sci. 106 (12), 3631–3641, 1.

Chiesa, E., Dorati, R., Modena, T., Conti, B., Genta, I., 2018. Multivariate analysis for the optimization of microfluidics-assisted nanoprecipitation method intended for the loading of small hydrophilic drugs into PLGA nanoparticles. Intern. j. pharm. 30 (1), 165–177, 536.

Chong, D., Liu, X., Ma, H., Huang, G., Han, Y.L., Cui, X., Yan, J., Xu, F., 2015. Advances in fabricating double-emulsion droplets and their biomedical applications. Microfluid. Nanofluidics 19 (5), 1071–1090.

Desai, K.G., Mallery, S.R., Schwendeman, S.P., 2008. Formulation and characterization of injectable poly (DL-lactide-co-glycolide) implant loaded with N-acetylcysteine, an MMP inhibitor. Pharmaceut. Res. 25 (3), 586–597.

Dheda, K., Gumbo, T., Maartens, G., Dooley, K.E., McNerney, R., Murray, M., Furin, J., Nardell, E.A., London, L., Lessem, E., Theron, G., 2017. The epidemiology, pathogenesis, transmission, diagnosis, and management of multidrug-resistant, extensively drug-resistant, and incurable tuberculosis. Lancet Respir. Med. 5 (4), 291–360, 1.

Du, W., Liao, L., Yang, L., Qin, A., Liang, A., 2017. Aqueous synthesis of functionalized copper sulfide quantum dots as near-infrared luminescent probes for detection of Hg 2+, Ag+ and Au 3+. Sci. Rep. 13 (1), 1–2, 7.

Ejigu, D.A., Abay, S.M., 2020. N-acetyl cysteine as an adjunct in the treatment of tuberculosis. Tubercul. res. treat. 30, 2020.

Emami, F., Yazdi, S.J., Na, D.H., 2019. Poly (lactic acid)/poly (lactic-co-glycolic acid) particulate carriers for pulmonary drug delivery. J. Pharm. Invest. 49 (4), 427–442.

Ezzati Nazhad Dolatabadi, J., Hamishehkar, H., Valizadeh, H., 2015. Development of dry powder inhaler formulation loaded with alendronate solid lipid nanoparticles: solid-state characterization and aerosol dispersion performance. Drug Dev. Ind. Pharm. 41 (9), 1431–1437, 2.

Guerini, M., Perugini, P., Grisoli, P., 2020. Evaluation of the effectiveness of N-acetylcysteine (NAC) and N-acetylcysteine-cyclodextrins multi-composite in Pseudomonas aeruginosa biofilm formation. Appl. Sci. 10 (10), 3466.

Iqbal, M., Zafar, N., Fessi, H., Elaissari, A., 2015. Double emulsion solvent evaporation techniques used for drug encapsulation. Intern. j. pharm. 30 (2), 173–190, 496.

Khadem-Hamedani, B., 2019. Design, Scale-Up and Optimization of Double Emulsion Processes. Doctoral dissertation, Lyon.

Khaira, R., Sharma, J., Saini, V., 2014. Development and characterization of nanoparticles for the delivery of gemcitabine hydrochloride. Sci. World J. 1, 2014.

Khatak, S., Mehta, M., Awasthi, R., Paudel, K.R., Singh, S.K., Gulati, M., Hansbro, N.G., Hansbro, P.M., Dua, K., Dureja, H., 2020. Solid lipid nanoparticles containing anti-tubercular drugs attenuate the Mycobacterium marinum infection. Tuberculosis 125, 102008, 1.

Lababidi, N., Montefusco-Pereira, C.V., de Souza Carvalho-Wodarz, C., Lehr, C.M., Schneider, M., 2020. Spray-dried multidrug particles for pulmonary co-delivery of antibiotics with N-acetylcysteine and curcumin-loaded PLGA-nanoparticles. Eur. J. Pharm. Biopharm. 157, 200–210, 1.

Labiris, N.R., Dolovich, M.B., 2003. Pulmonary drug delivery. Part II: the role of inhalant delivery devices and drug formulations in the therapeutic effectiveness of aerosolized medications. Br. J. Clin. Pharmacol. 56 (6), 600–612.

Lee, W.H., Loo, C.Y., Traini, D., Young, P.M., 2015. Nano-and micro-based inhaled drug delivery systems for targeting alveolar macrophages. Expet Opin. Drug Deliv. 3 (6), 1009–1026, 12.

Lin, J.J., Chen, J.S., Huang, S.J., Ko, J.H., Wang, Y.M., Chen, T.L., Wang, L.F., 2009. Folic acid–Pluronic F127 magnetic nanoparticle clusters for combined targeting, diagnosis, and therapy applications. Biomaterials 30 (28), 5114–5124, 1.

Mahajan, H.S., Gundare, S.A., 2014. Preparation, characterization and pulmonary pharmacokinetics of xyloglucan microspheres as dry powder inhalation. Carbohydr. Polym. 15, 529–536, 102.

Mahumane, G.D., Kumar, P., Pillay, V., Choonara, Y.E., 2020. Repositioning N-acetylcysteine (NAC): NAC-loaded electrospun drug delivery scaffolding for potential neural tissue engineering application. Pharmaceutics 12 (10), 934.

Makadia, H.K., Siegel, S.J., 2011. Poly lactic-co-glycolic acid (PLGA) is a biodegradable controlled drug delivery carrier. Polymers 3 (3), 1377–1397.

Mansur, H.S., Sadahira, C.M., Souza, A.N., Mansur, A.A., 2008. FTIR spectroscopy characterization of poly (vinyl alcohol) hydrogel with different hydrolysis degrees and chemically crosslinked with glutaraldehyde. Mater. Sci. Eng. C 28 (4), 539–548, 1.
Nasiruddin, M., Neyaz, M., Das, S., 2017. Nanotechnology-based approach in tuberculosis treatment. Tubercul. res. treat. 22, 2017.
Naveed, S., Amray, A., Waqas, A., Chaudhary, A.M., Azeem, M.W., 2017. Use of N-acetylcysteine in psychiatric conditions among children and adolescents: a scoping review. Cureus 9 (11).
Olsson, B., Johansson, M., Gabrielsson, J., Bolme, P., 1988. Pharmacokinetics and bioavailability of reduced and oxidized N-acetylcysteine. Eur. J. Clin. Pharmacol. 34 (1), 77–82, 1.
Organization Wh, 2020. *Global Tuberculosis Report* 2020. World Health Organization.
Parumasivam, T., Leung, S.S., Quan, D.H., Triccas, J.A., Britton, W.J., Chan, H.K., 2016. Rifapentine-loaded PLGA microparticles for tuberculosis inhaled therapy: preparation and *in vitro* aerosol characterization. Eur. J. Pharmaceut. Sci. 88 (10), 1, 1.
Prescott, L.F., Illingworth, R.N., Critchley, J.A., Stewart, M.J., Adam, R.D., Proudfoot, A.T., 1979. Intravenous N-acetylcysteine: the treatment of choice for paracetamol poisoning. Br. Med. J. 3 (6198), 1097–1100, 2.
Sanches, M.P., Gross, I.P., Saatkamp, R.H., Parize, A.L., Soldi, V., 2020. Chitosan-sodium alginate polyelectrolyte complex coating Pluronic® F127 nanoparticles loaded with citronella essential oil. J. Braz. Chem. Soc. 31 (4), 803–812.
Sharma, S., Parmar, A., Kori, S., Sandhir, R., 2016. PLGA-based nanoparticles: a new paradigm in biomedical applications. Trac. Trends Anal. Chem. 80 (1), 30–40.
Sharma, A., Vaghasiya, K., Gupta, P., Singh, A.K., Gupta, U.D., Verma, R.K., 2020. Dynamic mucus penetrating microspheres for efficient pulmonary delivery and enhanced efficacy of host defense peptide (HDP) in experimental tuberculosis. J. Contr. Release 324 (10), 17–33.
Singh, C., Bhatt, T.D., Gill, M.S., Suresh, S., 2014. Novel rifampicin–phospholipid complex for tubercular therapy: synthesis, physicochemical characterization, and in-vivo evaluation. Intern. j. pharm. 460 (1–2), 220–227, 2.
Singh, C., Koduri, L.S., Kumar, U.A., Bhatt, T.D., Kumar, V., Sobhia, M.E., Suresh, S., 2015a. Attenuation potential of rifampicin–phospholipid complex in murine hepatotoxicity model. J. Drug Deliv. Sci. Technol. 30, 225–231, 1.
Singh, C., Koduri, L.S., Singh, A., Suresh, S., 2015b. Novel potential for optimization of antitubercular therapy: pulmonary delivery of rifampicin lipospheres. Asian J. Pharm. Sci. 10 (6), 549–562, 1.
Singh, C., Koduri, L.S., Kumar, U.A., Bhatt, T.D., Kumar, V., Sobhia, M.E., Suresh, S., 2015 Dec 1. Attenuation potential of rifampicin–phospholipid complex in murine hepatotoxicity model. J. Drug Deliv. Sci. Technol. 30, 225–231.
Singh, C., Koduri, L.S., Bhatt, T.D., Jhamb, S.S., Mishra, V., Gill, M.S., Suresh, S., 2017. *In vitro-in vivo* evaluation of novel co-spray dried rifampicin phospholipid lipospheres for oral delivery. AAPS PharmSciTech 18 (1), 138–146.
Tafaghodia, M., Khademic, F., Shiehzadeha, F., Firouzia, Z., 2020. Polymer-based nanoparticles as delivery systems for treatment and vaccination of tuberculosis. In: Nanotechnology-Based Approaches for Tuberculosis Treatment, pp. 123–142.
Tripathi, A., Gupta, R., Saraf, S.A., 2010. PLGA nanoparticles of the anti-tubercular drug: drug loading and release studies of a water-insoluble drug. Int. J. Pharm. Tech. Res. 2 (3), 2116–2123.
Venkataraman, P., Herbert, D., Paramasivan, C.N., 1998. Evaluation of the BACTEC radiometric method in the early diagnosis of tuberculosis. Indian J. Med. Res. 108, 120–127.
Who, 2017. model List of Essential Medicines, twentieth ed. World Health Organization. https://doi.org/10.1016/S1473-3099(14)70780-7.
Winkler, J.S., Barai, M., Tomassone, M.S., 2019. Dual drug-loaded biodegradable Janus particles for simultaneous co-delivery of hydrophobic and hydrophilic compounds. Exp. Biol. Med. 244 (14), 1162–1177.
Yoo, J., Won, Y.Y., 2020. Phenomenology of the initial burst release of drugs from PLGA Microparticles. ACS Biomater. Sci. Eng. 9 (11), 6053–6062, 6.
Yudhawati, R., Prasanta, N., 2020. The role of N-acetylcysteine in pulmonary tuberculosis. J. Respirasi. 30 (1), 27–34, 6.
Zakeri-Milani, P., Loveymi, B.D., Jelvehgari, M., Valizadeh, H., 2013. The characteristics and improved intestinal permeability of vancomycin PLGA-nanoparticles as colloidal drug delivery system. Colloids Surf. B Biointerfaces 103, 174–181, 1.
Zarchi, A.A., Abbasi, S., Faramarzi, M.A., Gilani, K., Ghazi-Khansari, M., Amani, A., 2015. Development and optimization of N-Acetylcysteine-loaded poly (lactic-co-glycolic acid) nanoparticles by electrospray. Int. J. Biol. Macromol. 72 (1), 764–770.
Zhao, T., Liu, Y., 2010. N-acetylcysteine inhibit biofilms produced by Pseudomonas aeruginosa. BMC Microbiol. 10 (1), 1–8.